COBEM 2023 27TH INTERNATIONAL CONGRESS OF MECHANICAL ENGENEERING

ABCM Brazilian Society of Mechanical Sciences and Engineering
27th ABCM International Congress of Mechanical Engineering
December 04-08, 2023, Florianópolis-SC, Brazil

COB-2023-1090
INVESTIGATION ON THE USE OF PARALLEL FOUR-BAR LINKAGES IN HUMANOID ROBOT LEGS DURING STAND-UP MOTION

Thiago Rodrigues de Oliveira Tonaco
Thiago de Paula Sales
Aeronautics Institute of Technology, Praça Mal. Eduardo Gomes, 50, Vila das Acácias, ZIP 12228-900, São José dos Campos – SP – Brazil
tonaco.k.t22@gmail.com, tpsales@ita.br

Abstract. *Humanoid robots might be required to perform a stand-up motion, to recover their natural stance and continue to perform tasks, when balance is lost for some reason. Stand-up procedures might demand quite an effort from actuators, which might fail if not properly designed. Within this context, authors aim to compare two different designs for a humanoid robot leg, and their influence on loads required for actuation. The first type of leg corresponds to a serial arrangement of rigid links, while the alternative comprises the use of parallel four-bar linkages in place of the rigid bodies connecting ankle and knee, and the knee to the hip. The baseline robot one considers has been designed to participate in the RoboCup Humanoid League competition. The robot kinematic chain is modeled as a multibody system, using the SimScape platform. Through a kinematic analysis, the angles of the ankle and knee joints are determined from the motion specified for the hip. Different stand-up motions are considered, and their influence on actuation is considered. Results show that the use of four-bar linkages in the robot's legs can better distribute actuation requirements, which can be desired in several humanoid robot applications.*

Keywords: *humanoid robot, mechanical design, four-bar linkage, multibody dynamics.*

1. INTRODUCTION

In the recent past, the field of legged robotics has gained attention from both academic and industry communities. To exemplify interest on the matter, one can inspect developments made by Boston Dynamics, related to the robots ATLAS and Spot (Boston Dynamics, 2023a,b). In this context, many robotics' competitions have been established, to encourage growth of the field. One of them is RoboCup, which encompasses the Humanoid KidSize League: in it, teams composed of four humanoid robots play soccer against each other, aiming to win the championship (RoboCup Federation, 2023).

The team "ITAndroids", from the Aeronautics Institute of Technology (ITA), usually participates in such competitions. For the Humanoid KidSize League, and also aiming towards research activities, it has developed the "Chape.G1" robot. It is relatively small, with a height of 53 cm, having been fully designed at ITA — with the robot's original design being based on the open source project Robotis OP2 robot (Ha *et al.*, 2013).

Initial versions of the Chape.G1 project, which can be seen in Fig. 1a, proved to be satisfactory. Nevertheless, some issues have been found with it, arising from the nature of the adapted design, or the (lack of) manufacturing capability by the team. While the robot's mechanical design has been developed and improved over the years, some problems still persist with it.

For instance, one is that servomotors located in the robot's knee joints tend to experience more frequent damage than those used elsewhere. In terms of cost, failure of servomotors is very significant: the Chape.G1 project makes use of 20 servomotors, which represent approximately 80 % of the overall cost of a unit.

Two types of damage can be seen to occur with the motors used in the robots: mechanical and electronic. Mechanical damage is relatively low-cost to maintain, as it usually involves replacing some broken internal gears. Electronic damage, on the other hand, typically occurs when the electric current exceeds limits which can be handled by the servomotor's electronic boards, resulting in short-circuit, and necessitating the replacement of the damaged motor. The reduction of failures, especially of the latter kind, is therefore highly desirable.

Currently, the team responsible for producing the Chape.G1 robot has been creating a new, larger robot, designated "Chape.G2", with an expected height of 70 cm. While the digital model of this robot has been finalized (Tonaco *et al.*, 2020), which can be seen in Fig. 1b, it has not been fully manufactured yet. One of the goals with the development of this new robot has been to solve issues observed with the Chape.G1 project, such as the one related to servomotors used in the knee joints.

To tackle this problem, a possible approach is to improve the distribution of required torques between the servomotors used in each leg, through the implementation of a new leg configuration, encompassing four-bar linkages. Presently, the Chape.G2 design features the same leg arrangement which is used by the Chape.G1 robot, with links placed in series.

The proposed solution strategy has been inspired by the mechanical arrangement found in the GankenKun robot, which can be seen in Fig. 1c. It has been developed by a Japanese team (CIT Brains, 2023), which also participates in RoboCup. This robot uses four-bar linkages in its legs, as can be seen in Fig. 1d. This mechanism allowed the team to use Kondo B3M-SC-1170-A servomotors, which are less powerful than the XM540-W150-T/R servomotors from Robotis, planned to be used in the legs of the Chape.G2 model. The four-bar linkage system was employed to decrease the amount of power required by the knee servomotor, by distributing the load with other motors used in the robot's legs.

This approach is supported by results shown in other works. For example, Sancisi *et al.* (2009) discuss the importance of an optimized design for lower limb prostheses, particularly knee devices. As the authors discuss, four-bar linkages, although simple, are the most adopted arrangement for knee joints, as they are able to provide sufficient stability and can reproduce natural knee motion with reasonable accuracy.

Within this context, in this article we aim to evaluate the effectiveness of adopting four-bar mechanisms in the legs of a humanoid robot — namely, for the Chape.G2 robot, which takes central role in our case study. To meet this goal, we perform numerical simulations, relying on a multibody dynamics rationale. Analyses are performed to verify the proper functioning of the investigated leg geometry. We believe that other researchers working with humanoid robotics can benefit from the proposed leg design, as well as of the design process described in here.

The remainder of this article is organized as follows. In Section 2, the methodology employed in this work is presented. Obtained results are shown and discussed in Section 3. Finally, summary and conclusions are drawn in Section 4.

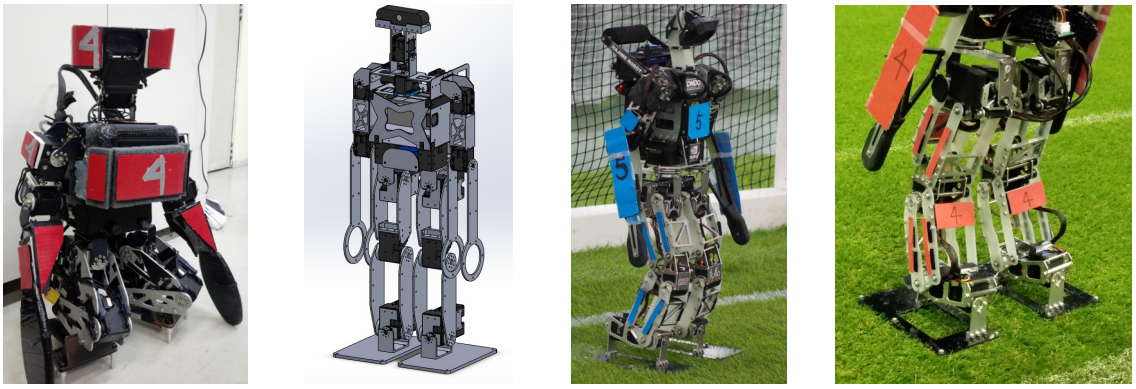

(a) Chape.G1 robot. (b) Chape.G2 CAD model. (c) GankenKun robot. (d) GankenKun robot's leg.

Figure 1: Examples of humanoid robots which participate in the RoboCup competition.

2. METHODODOLOGY

Based on what has been shown by Tonaco *et al.* (2019), the motion which most demands torque from servomotors on the legs of a humanoid robot is the one during which the robot has to stand up. Because of this, during the developed research, only this type of motion has been considered for setting up simulations. The rising up motion was determined taking as reference what is currently executed by the Chape.G1 robot, as well as motion exhibited by robots of the Japanese team CIT Brains. These are compared by means of snapshots in Fig. 2. The stand-up motions of the Chape.G1 and GankenKun-OP robots last approximately 3 s and 1 s, respectively.

We consider the stand-up motion starts when the robots' arms lose contact with the ground. The main aspect which deserves attention from the presented data is related to the location of the robots' centers of mass during the motion. In Fig. 3, one has highlighted the initial and final positions of the centers of mass, as well as kinematic joints, and vertical lines, which pass through the main support points on the robots' feet.

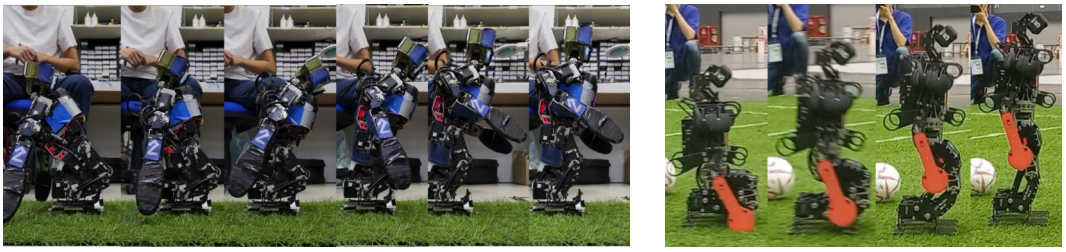

(a) Chape.G1 standing up. (b) GankenKun-OP standing up.

Figure 2: Still frames of the stand-up motions executed by distinct robots.

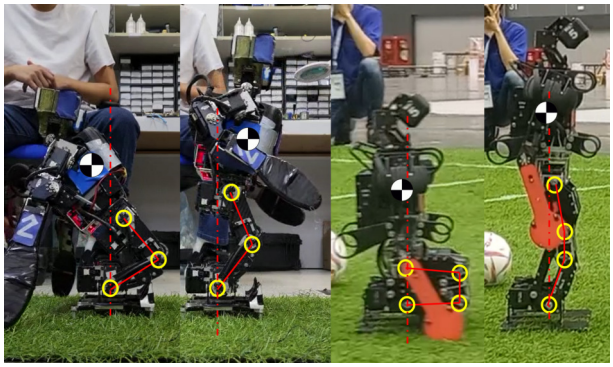

Figure 3: Approximate locations of the centers of mass of the considered robots during their stand-up motions.

It can be seen that the center of mass of the Chape.G1 robot oscillates around the drawn vertical line. This implies that motors on the knee have to spend more energy to maintain the Chape.G1 robot balanced and standing up. Another observation is related to the conservation of momentum: after the center of mass reaches the drawn vertical line, it continues its motion towards the right, in the figure; this inertia driven load has to be counteracted upon by the motors, implying in increased energetic expense.

On the other hand, the CIT Brains team's robot maintains its center of mass more stable during the stand-up motion, without it appearing to possess any significant horizontal component. This, in comparison, should lead to smaller energy and torque requirements to perform the required motion. Clearly, a pure vertical motion of the robot center of mass is most desirable while it stands up.

2.1. Geometry of the analyzed legs and position analysis

Here, one considers two different leg models. The first one is denoted "simple leg" (PS), corresponding to the one used in the Chape.G1 robot; while the second one is named "four-bar model" (4B). Both geometries can be seen in Fig. 4.

Let θ_2 be the angle that the lower structure of the leg in the PS model, Fig. 4a, represented by the line segment $\overline{OA}$, with length r_2, makes with the ground. Also, let θ_3 be the angle that the line segment $\overline{AB}$ makes with the horizontal. Other angles of interest are the opening angles between the links, as these are the joint angles, that the servomotors must change, denoted as Θ_2 and Θ_3. The angle Θ_2 is equal to θ_2, while $\Theta_3 = \pi - \theta_3 + \theta_2$. Representing a position vector as $\overrightarrow{OB} = \mathbf{r}_1$ in terms of its x and y components, we can write:

$$\overrightarrow{OA} = \mathbf{r}_2 = r_2 \begin{Bmatrix} \cos(\Theta_2) \\ \sin(\Theta_2) \end{Bmatrix}; \qquad \overrightarrow{AB} = \mathbf{r}_3 = r_3 \begin{Bmatrix} -\cos(\Theta_2 - \Theta_3) \\ -\sin(\Theta_2 - \Theta_3) \end{Bmatrix}; \qquad \mathbf{r}_1 = \mathbf{r}_2 + \mathbf{r}_3. \tag{1}$$

A similar analysis can be done for the 4B leg, while taking into account the part which separates its upper and lower portions. One highlights that, for the 4B leg, the opening angle of the knee is given $\Theta_3 = \pi - \theta_3$, as observed in Fig. 4b. With regard to vectors, they are given by:

$$\overrightarrow{CB} = \mathbf{r}_3 = r_3 \begin{Bmatrix} -\cos(\Theta_3) \\ \sin(\Theta_3) \end{Bmatrix}; \qquad \overrightarrow{AB} = \mathbf{r}_k = r_k \begin{Bmatrix} 0 \\ 1 \end{Bmatrix}; \qquad \mathbf{r}_1 = \mathbf{r}_2 + \mathbf{r}_3 + \mathbf{r}_k. \tag{2}$$

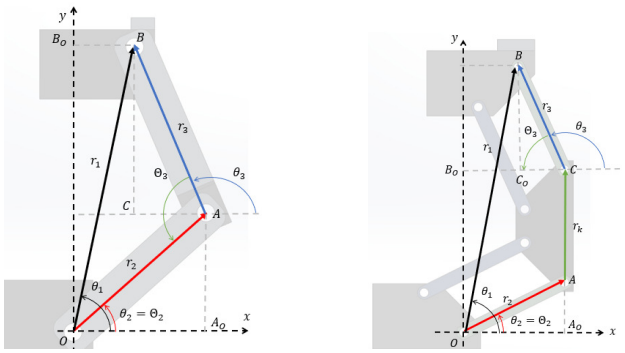

(a) Simple leg model. (b) Four-bar (4B) model.

Figure 4: Geometric aspects of the legs considered in this work.

Based on the previous expressions, by specifying a position for B, we can compute the values required for Θ_2 and Θ_3 — so that B can be located appropriately. This kinematic inversion is employed by us, since the stand-up motion simulations we perform have been done by imposing $y = y(t)$ — with y the vertical position of B. While the inverse-kinematics model can be developed analytically, tasks leading to it were performed using symbolic algebra software.

2.2. Types of movements

In this work, one always assumed x (the horizontal location of B) to be constant over time, equal to its initial value. For y, four different types of movements were considered: cycloidal, simple harmonic, modified trapezoidal, and linear. This strategy was adopted to evaluate the influence of the input motion on power and torque requirements of the servomotors. Thus, the value of $y = y(t)$ follows what is shown in Tab. 1. In its first row, y_0 denotes the initial vertical location of B, and h represents the motion range which should be traveled by B. The normalized time $\tilde{t}$ is given by $(t - t_0)/T$, with t being the physical time, t_0 the time instant when the motion starts, and T the motion duration.

Table 1: Vertical motions prescribed to point B.

Movement type	Function $[y(t) - y_0]/h$
Cycloidal (*cy*)	$\tilde{t} - \sin(2\pi\tilde{t})/(2\pi)$
Simple harmonic (*shm*)	$[1 - \cos(\pi\tilde{t})]/2$
Modified trapezoidal (*trap*)	$\begin{cases} 9\tilde{t}^2/4, & \text{if } 0 \le \tilde{t} < 1/3 \\ 3\tilde{t}/2 - 1/4, & \text{if } 1/3 \le \tilde{t} < 2/3 \\ 1 - 9(1-\tilde{t})^2/4, & \text{if } 2/3 \le \tilde{t} \le 1 \end{cases}$
Linear	$\tilde{t}$

2.3. CAD models and servomotor operational limits

Figure 5 shows a perspective view of the Chape.G2 geometry, with sub-assemblies of interest being highlighted. These comprise the ankle, knee, and lower and superior leg structures. In Table 2, the mass of each of these is summarized.

Of particular interest for the analyses performed by us, are the specifications of the servomotors used in the legs of the Chape.G2 robot. These are XM540-W150-T/R servomotors (abbreviated XM540), which are manufactured by a

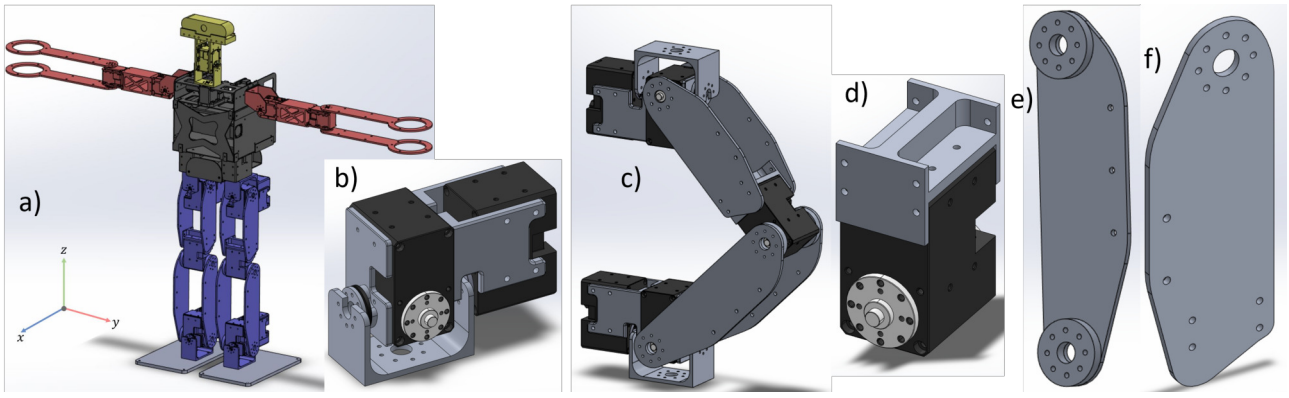

Figure 5: Complete Chape.G2 CAD model, in a), and some of its sub-assemblies: b) ankle; c) “simple leg”; d) knee; e) lower leg structure (LLS) component; and f) superior leg structure (SLS) component.

Table 2: Approximate masses of the different legs considered for the Chape.G2 robot, and of their sub-assemblies.

Robot leg type	Total leg mass (g)	Ankle mass (g)	LLS mass (g)	Knee mass (g)	SLS mass (g)
Simple (PS)	1181.83	358.07	169.28	200.88	95.52
Four-bar (4B)	1300.43	372.63	148.05	259.08	148.05

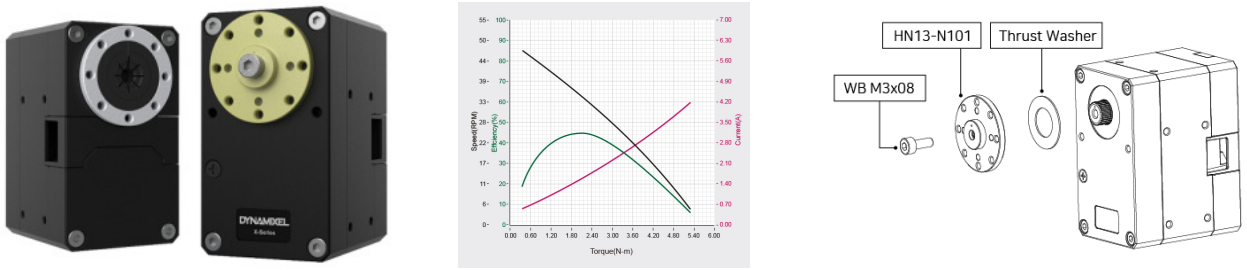

(a) Photographs showing the servomotor. (b) Performance curves. (c) Actuator horn assembly.

Figure 6: XM540-W150-T/R servomotor.

South-Korean company (ROBOTIS, 2023a,b). Figure 6 shows photographs of the actual device, together with a plot which includes the actuator speed versus torque curve, and a drawing showing how the actuator horn can be assembled, with the help of a thrust washer, to the output shaft of the servo. The XM540 has a mass of 165 g, a stall torque of 7.3 N m, and maximum revolution speed of 5.55 rad/s. One should also point out that it only has one torque-generating output shaft, on one of its faces.

For protection, the servomotors have a contingency system based on the electrical current value: if it is larger than the allowable limit, and tries to flow through the circuits of a servomotor, it will shut down to prevent damage to its components, such as its control board. This type of occurrence gradually damages a servomotor — even if it continues to function, a recurrence of similar events can wear out the motor to the point where the contingency process no longer works, leading to a definitive failure of the servomotor. In such cases, replacement of the entirety of a servomotor becomes necessary.

A prototype of the Chape.G2 robot with its legs replaced by new ones, incorporating parallel four-bar linkages, was developed for conducting this research, in CAD environment. Figure 7 shows the new design, as well as some sub-assemblies and parts. Masses of the components of the "four-bar leg" have been recorded in Table 2, presented previously.

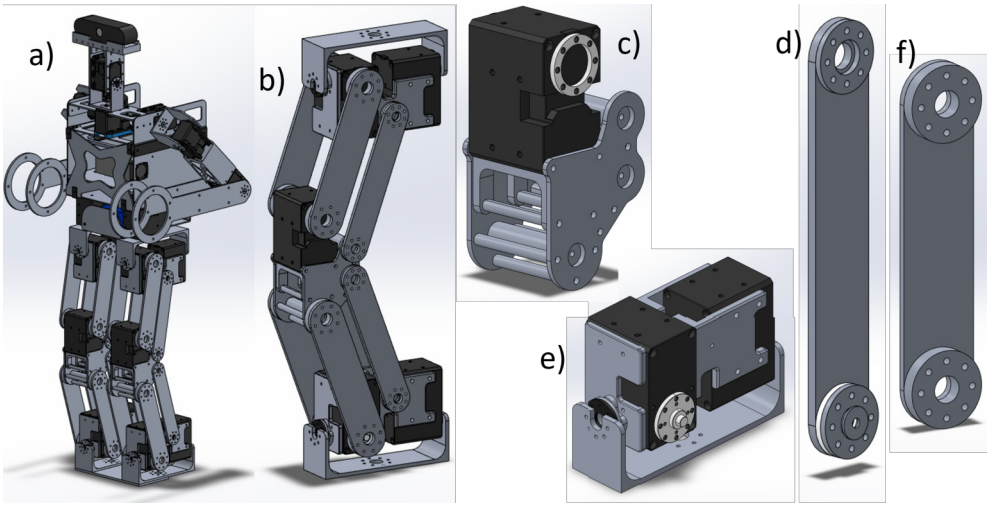

Figure 7: CAD model of the Chape.G2 robot with legs incorporating parallel four-bar linkages, in a), and some sub-assemblies and components: b) 4B leg; c) knee; d) front piece of leg structures; e) ankle; f) rear piece of leg structures. Parts d) and f) are used in both SLS and LLS of the 4B leg.

By comparing the prototype leg displayed in Fig. 7 with the one from the Japanese GankenKun robot, seen in Fig. 1c, we can observe that the adopted structural arrangements are very similar, resembling a sort of "cage". In this respect, the main differences between both projects are that the Japanese robot already features parts that have been topologically-optimized, and that it has an additional degree of freedom in each of its feet, allowing them to rotate, despite the geometric arrangement of its legs.

2.4. Computational physical models

Physical models of the Chape.G2 robot with simple and four-bar legs were constructed in the `MATLAB/Simulink` software, exploring the multibody dynamics capabilities of the `SimScape` tool. To achieve this, a feature of the employed CAD software was explored, which allows exporting an `XML` file for a virtual assembly. Generated `XML` files were then imported and converted into physical models in the `Simulink/SimScape` environment.

In Fig. 8a, one shows how the generated `Simulink/SimScape` block diagrams look, after they have been organized, and augmented with a subsystem developed to apply prescribed motions to the hip point B, cf. Table 1. The `motion_function` block diagram is shown in Fig. 8b: it essentially consists of a `MATLAB` function that determines how the leg movement must occur. The input variables of the function are time (t), the prescribed type of movement (k), the duration of the motion (`duracao`, equivalent to T), and the instant at which it initiates (`t_inicio`, or t_0 in the definition of $\tilde{t}$). The function provides as outputs: Θ_2 (`TH2`), Θ_3 (`TH3`), and the position (x, y) of the upper ankle revolute joints, where B is located.

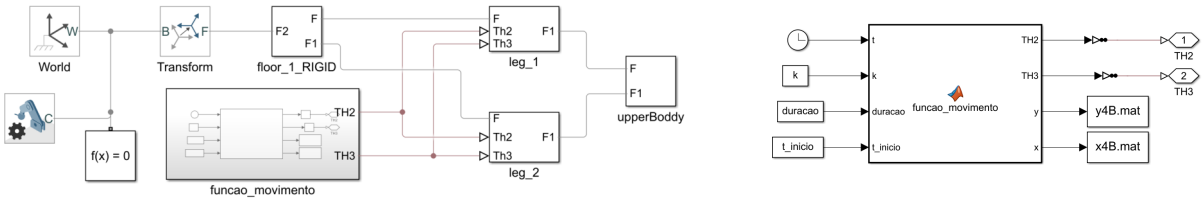

(a) General block diagram.

(b) Diagram of the `motion_function`.

Figure 8: `Simulink/SimScape` block diagrams for the analyzed robots.

If one accesses the subsystem related to one of the legs of the robots, one is greeted with the block diagrams shown in Fig. 9. These clearly portray the topology of the mechanical arrangement of bodies in the analyzed legs. Individual blocks seen in Fig. 9 have been named according to the terminology introduced in Figs. 5 and 7.

To make simulations more akin to reality, two considerations were made. First, since the adopted servomotors only generate torque and motion on one of their sides, only one side of each leg has the values of Θ_2 and Θ_3 prescribed, with the other being passive. Second, one desired to keep the upper ankle parallel to the lower one, in order to make the UpperBody of the robot vertical with respect to the ground, throughout all the stand-up motion. This requires a parallelism constraint in the model of the robot equipped with "simple legs", as can be seen from Fig. 9a. In the case of the legs made with parallel four-bar linkages, this is not necessary, due to underlying geometric characteristics.

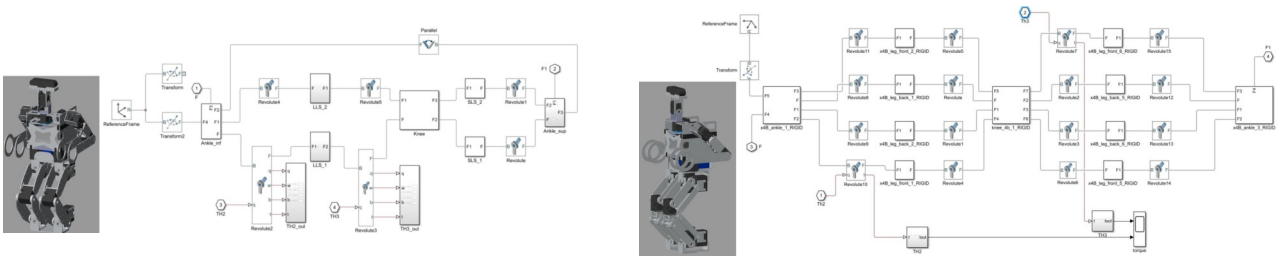

(a) Chape.G2 robot with simple legs.

(b) Chape.G2 robot with legs with parallel four-bar linkages.

Figure 9: `Simulink/SimScape` block diagrams for the distinct analyzed leg types, as well as 3D visualization of the models in the simulation environment.

Finally, before presenting results, one should point out that all bodies have been considered rigid. Also, friction effects, contact, and free-play have been neglected. Gravity acted on the vertical direction. Inertia of the actuators, while possibly being very relevant, has not been taken into account, as data was not found for the polar moment of inertia of the motors.

3. RESULTS AND DISCUSSION

All prescribed motions analyzed in the following have the same duration, of 1 s, which is similar to the one observed for the Gankenkun-OP robot. The reason for this choice is that faster motions should require larger power levels from the servomotors to execute them.

Numerical integration was performed using the `ode15s` routine, while adopting a 1×10^{-6} relative tolerance threshold.

The results which are presented first are related to kinematics, in Fig. 10. Regarding angular positions, the main and most important difference lies in the angular variation throughout the movement between the models. The angular variation of Θ_2 does not differ much between the PS and 4B models, with the only significant difference being the initial

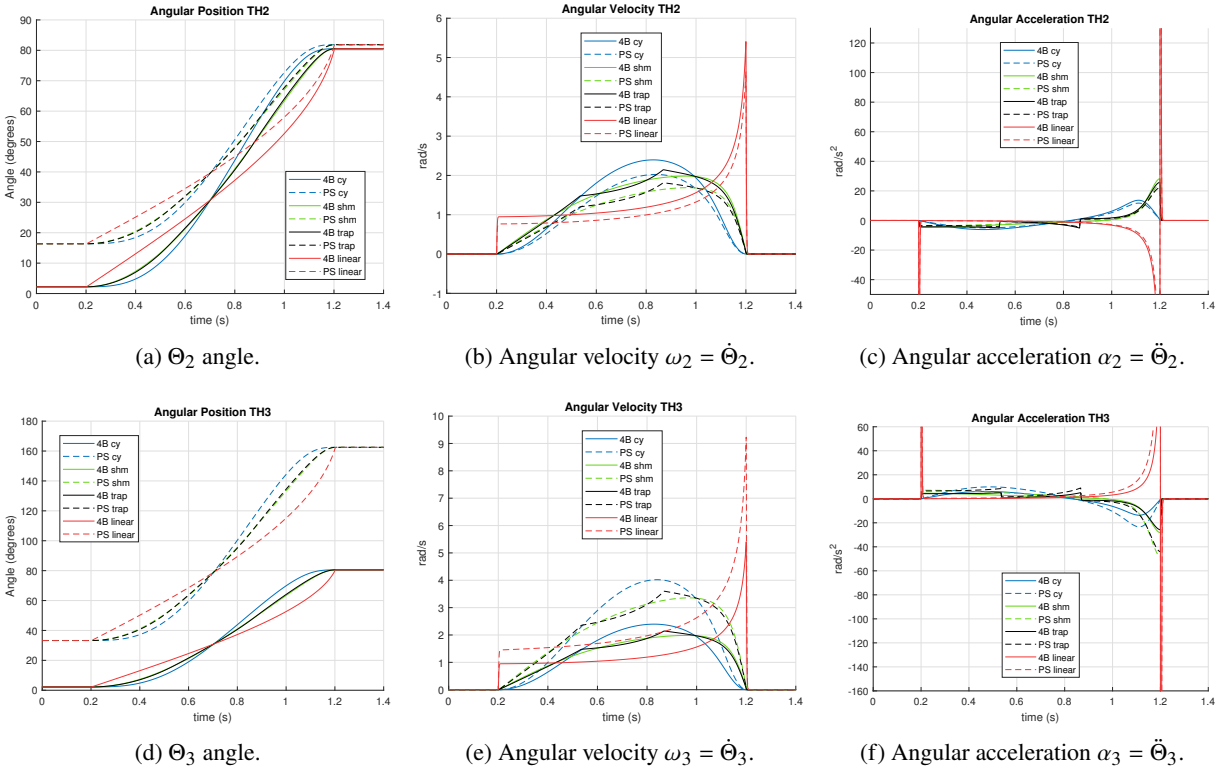

(a) Θ_2 angle. (b) Angular velocity $\omega_2 = \dot{\Theta}_2$. (c) Angular acceleration $\alpha_2 = \ddot{\Theta}_2$.

(d) Θ_3 angle. (e) Angular velocity $\omega_3 = \dot{\Theta}_3$. (f) Angular acceleration $\alpha_3 = \ddot{\Theta}_3$.

Figure 10: Angular positions, velocities and accelerations of the legs' joints, for all input motion types.

value, which is justified by the different geometry of the models. On the other hand, the angular variation of Θ_3 between the models is more significant. It can be observed that the angular variations of Θ_3 and Θ_2 in the 4B model are exactly the same: both exhibit the same behavior, spanning 80° between initial and final configurations. On the other hand, for the simple leg model, the angle Θ_3 varies more than 120° from its starting value up to its final value.

The angular velocities $\omega_2 = \dot{\Theta}_2$ and $\omega_3 = \dot{\Theta}_3$ exhibit behaviors similar to the velocities of the specified movements for point B. If its motion is continuous, angular velocities of the joints are expected to also be continuous. If the motion presents discontinuities or kinks, corresponding velocities should also present anomalies. For instance, the angular velocities associated with cycloidal and simple harmonic motions exhibit continuous behavior. Results from simulations with modified trapezoidal motion show, on the other hand, distinct features associated with time instants $t = 0.2\,\mathrm{s} + T/3$ and $t = 0.2\,\mathrm{s} + 2T/3$, which correspond to the segmented portions of the function, justifying the non-differentiability of the calculated velocities. For linear prescribed motion, initially, zero velocities are observed, but they suddenly experience jumps indicative of discontinuities. These are followed by continuous behavior until the end of the motion, when jumps are observed again, with velocities returning to zero. These observations hold true for all simulations. One important point to note is that in the 4B model, the angular velocities ω_2 and ω_3 have the same absolute value at a given time instant, with their signs differing only due to the opposite rotation directions. This fact is consistent across all simulations.

An analysis of the angular accelerations of the leg parts was conducted to characterize their behavior and facilitate the interpretation of other results. For the linear prescribed motion, angular accelerations exhibited two peaks/jumps, at the beginning and end of the motion, due to abrupt changes in angular velocities at such instants. For the cycloidal function, smooth angular accelerations are observed, being differentiable at all points, and having zero accelerations at the beginning and end of the motion. In simulations considering simple harmonic motion, angular accelerations are differentiable at all times, except when the motion starts or ends, instants at which jumps occur, indicating non-smooth transitions. In the case of the modified trapezoidal function, the angular accelerations exhibit a behavior similar to simple harmonic motion, with jumps at the beginning and end. Two additional time instants can be seen to be associated with non-differentiability of angular velocities. Based on this analysis, one decided to not continue investigating simulations considering applied linear motion, as it would lead to torque and power values much larger than any servomotor would withstand.

Torque values for the other motions can be visualized in Figures 11a and 11b. Similar behaviors to those observed for angular accelerations can be noticed in terms of continuity and differentiability. When analyzing the torques required for actuation in the simulations, there is an apparent disparity in values between the model with simple legs and the servomotors driving the ankle and knee joints of the leg (angles Θ_2 and Θ_3). The joint associated with angle Θ_2 requires significantly smaller torques compared to the joint associated with angle Θ_3. On the other hand, the torque values in the simulations of the robot equipped with four-bar linkages in its legs are quite close to each other. This indicates a

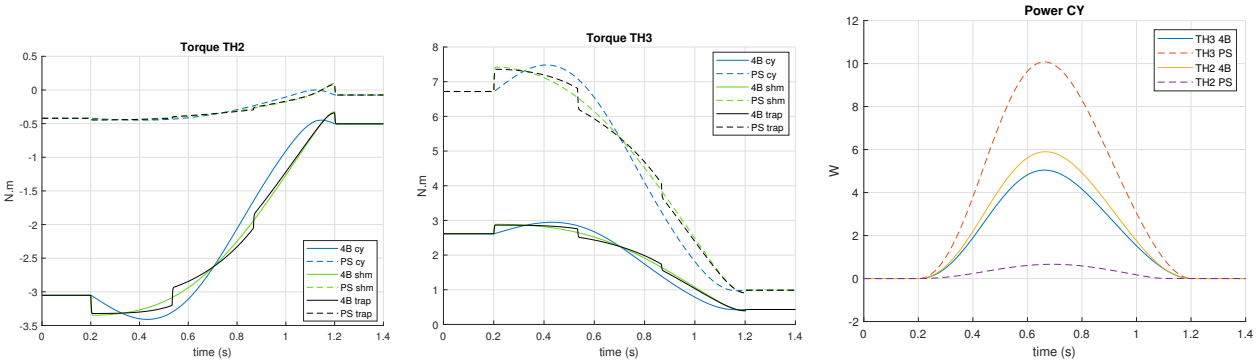

(a) Reaction torque associated with Θ_2. (b) Reaction torque associated with Θ_3. (c) Required powers for cycloidal motion.

Figure 11: Comparison of torques and power required for realization of the prescribed stand-up motions by the robots with simple legs and parallel four-bar linkages legs.

clear balance in the torque application by the actuators in the 4B leg, which is due to the specific geometry of the leg, incorporating four-bar mechanisms.

This last statement becomes clearer when power requirements are compared, as shown in Fig. 11c for one of the considered prescribed motions. The power values associated with the simple legs are disproportionate between the actuators, specially when those related to the alternative leg arrangement are considered. For the first model, the power required to actuate Θ_2 is small (less than 1 W), while it is large for Θ_3 (almost 10 W). For the model with four-bar linkage legs, the power requirement is much more balanced (5.2 W for Θ_2 and 4.8 W for Θ_3). These observations are partly due to the larger angular displacement experienced by Θ_3 in the model with simple legs. In the 4B model, Θ_2 handles more load. This shows that the model utilizing four-bar mechanisms distributes power requirements for the lifting motion more efficiently between the actuated joints.

To verify if XM540 servomotors used in the Chape.G2 robot are capable of providing the required actuation effort, the plot presented in Fig. 6b was used as a reference. Curves were constructed showing the variation of angular velocity as a function of the required torque for the actuator. Results are shown in Fig. 12. It is evident that the main difference between the models is the balance of requirements for the actuators in the 4B model, while a difference in demands are observed for the joints of the model with simple legs. For the 4B model, results keep within the operating limits of the XM540 servomotor, while those related to the other model exceed the motor capacity. Therefore, the proposal of a leg design which incorporates parallel four-bar mechanisms is seen to be feasible and advantageous in terms of the investigation performed herein. The considered design can be useful for undergraduate teams which participate in the RoboCup competition, such as ITAndroids.

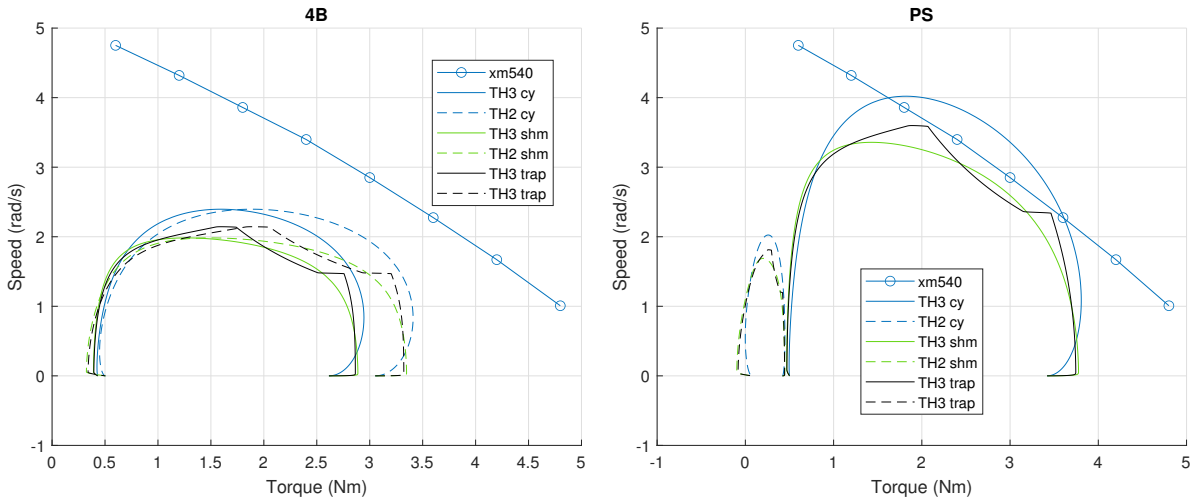

(a) Speed versus torque plot associated with 4B. (b) Speed versus torque plot associated with PS.

Figure 12: Angular velocity versus required torque for actuation.

4. CONCLUSIONS AND FUTURE WORK

In this paper, one studied how the adoption of four-bar linkages in humanoid robots' legs can benefit actuation requirements, in terms of demanded torques and powers, during standing-up motions. By means of numerical simulations, the feasibility of the investigated design has been demonstrated, since requirements for actuation showed to be better distributed between actuators for the leg design equipped with parallel four-bar linkages. For arriving at such conclusion, we remember one initially compared the stand-up motions of a couple of robots, which helped justify our approach. After this, one developed CAD models, based on which physical models were constructed in the `Simulink/SimScape` simulation environment. Different prescribed motions were considered for analyses, as one has not taken into account electromechanical couplings which exist in an actual robot, responsible for several control loops of the hardware.

Several simplifications have been made when one developed models and conducted simulations. Nevertheless, we believe our main conclusion should hold even if some of them are uplifted. Our view is that the finding we report is mainly due to the geometric arrangement of the investigated legs.

Several future avenues for research can be listed with regard to the work presented in this study. To name a few: validation of numerical findings through experimental tests; to evaluate the influence of flexible robot components on the performance of analyzed leg mechanisms; to incorporate algorithms used to control humanoid robot motion in the simulations; analysis of the effects that joint clearances and friction have on actuation precision and control; to optimize components to enhance rigidity and decrease mass in the robot legs; to determine optimal servomotor movement; to model servomotors as electromechanical systems; and to assess the performance of the proposed leg design across various robot movements.

5. REFERENCES

Boston Dynamics, 2023a. "ATLAS". URL `https://www.bostondynamics.com/atlas`.

Boston Dynamics, 2023b. "Spot". URL `https://www.bostondynamics.com/products/spot`.

CIT Brains, 2023. "Go beyond humans in soccer". URL `https://citbrains.studio.site/en`.

Ha, I., Tamura, Y. and Asama, H., 2013. "Development of open platform humanoid robot DARwIn-OP". *Advanced Robotics*, Vol. 27, No. 3, pp. 223–232. doi:10.1080/01691864.2012.754079.

RoboCup Federation, 2023. "RoboCup Humanoid League: Rules". URL `https://humanoid.robocup.org/materials/rules/`.

ROBOTIS, 2023a. "The study of human experiences, ROBOTIS". URL `http://en.robotis.com/`.

ROBOTIS, 2023b. "XM540-W150-T/R". URL `https://emanual.robotis.com/docs/en/dxl/x/xm540-w150/`.

Sancisi, N., Caminati, R. and Parenti-Castelli, V., 2009. "Optimal four-bar linkage for the stability and the motion of the human knee prostheses". In *Atti del XIX CONGRESSO dell'Associazione Italiana di Meccanica Teorica e Applicata*. URL `https://www.dipmat.univpm.it/aimeta2009/AttiCongresso/MECCANICA_MACCHINE/parenti_paper268.pdf`.

Tonaco, T., Faria, D.V., Silva, C., Maximo, M. and Arbelo, M., 2019. "Humanoid robot leg design". In *Proceedings of the 25th International Congress of Mechanical Engineering*. ABCM. doi:10.26678/ABCM.COBEM2019.COB2019-1595.

Tonaco, T.R.O., Silva, C.C.D. and Arbelo, M.A., 2020. "Projeto mecânico de um robô humanoide". In *Anais do XXVI Encontro de Iniciação Científica e Pós-Graduação do ITA – XXVI ENCITA*. Instituto Tecnológico de Aeronáutica.

6. RESPONSIBILITY NOTICE

The authors are solely responsible for the printed material included in this paper.